ELSEVIER

Carbohydrate Polymers 47 (2002) 109–119

Carbohydrate Polymers

www.elsevier.com/locate/carbpol

NMR velocity imaging of the flow behaviour of hyaluronan solutions

S.G. Harding[a,*], O. Wik[b,c], A. Helander[b], N.-O. Ahnfelt[b], L. Kenne[a]

[a]*Department of Chemistry, Swedish University of Agricultural Sciences, Arrheniusplan 8, P.O. Box 7015, SE-750 07 Uppsala, Sweden*
[b]*Pharmacia and Upjohn AB, SE-751 82 Uppsala, Sweden*
[c]*Q-Med, SE-752 28 Uppsala, Sweden*

Received 4 April 2000; accepted 14 August 2000

Abstract

Hyaluronan (hyaluronic acid) solutions are widely used in medicinal applications due to their biological compatibility and rheological properties. This work uses the technique NMR velocity imaging to study the flow behaviour of hyaluronan solutions pumped through Teflon tubing. Three commercially available hyaluronan solutions, (Healon®, Healon® GV and Healon®5) were investigated along with a set of samples with concentrations ranging from 1 to 23 mg ml^{-1} and weight average molecular weight, $\bar{M}_w$, between 0.3 and 5.2×10^6. The shape of the velocity profiles were found to vary significantly with $\bar{M}_w$, concentration and apparent shear rate. Transitions were observed from near Newtonian flow to shear thinning to wall slip with increasing $\bar{M}_w$ and concentration. Solutions with the highest $\bar{M}_w$ and concentration showed possible 'shear banding' effects in addition to wall slip with a distinctive region of high shear with an annulus of around 50 μm at the edge of the tube.

Keywords: NMR imaging; Rheology; Pipe flow; Wall slip; Shear banding; Hyaluronic acid; Hyaluronan; Entangled polymers

1. Introduction

The aim of this study is to investigate the flow behaviour of hyaluronan solutions under shear. The velocity distribution of the solution as it flows through Teflon (PTFE) tubing is measured using the technique of Nuclear Magnetic Resonance (NMR) velocity imaging. NMR velocity imaging has significant advantages over conventional rheometry in that the flow curve (shear stress against strain rate) that characterises the fluid can be measured in a model independent way and surface phenomena and flow hysteresis can be directly visualised. An understanding of the behaviour of these interesting biomaterials under shear is important from both a theoretical view-point to further our knowledge of the entanglement dynamics of random coil polymers in solution and from a practical view-point to develop their medical applications.

Hyaluronan is a naturally occurring bio-compatible linear polysaccharide, that forms aqueous solutions with complex rheological character (AlAssaf, Meadows, Phillips & Williams, 1996; Ambrosio, Borzacchiello, Netti & Nicolais, 1999; Bothner & Wik, 1989; Bothner, Waaler & Wik, 1988; Desmedt, Dekeyser, Ribitsch, Lauwers & Demeester, 1993; Milas, Roure & Berry, 1996). Hyaluronan is made up of repeating disaccharide units of *N*-acetylglucosamine and sodium glucuronate linked by β1-3 and β1-4 glycosidic bonds. The molecular mass of hyaluronan is typically 1–10 million. In solution the molecules assume a stiffened expanded random coil structure, due to the limited freedom of rotation of the glycosidic bonds.

Hyaluronan is widely distributed in animal tissues and is also produced by some bacteria. Especially high concentration of hyaluronan is found in soft connective tissues such as the synovial fluid and the vitreous humour of the eye. It is present in the extracellular matrix of all tissues of all species. As a result of its biological compatibility and rheological properties it is already used in several biomedical applications and an increasing number of potential applications are currently being explored. In particular, hyaluronan is widely used as an ophthalmosurgical aid in for example, cataract and trauma surgery, corneal transplantation and glaucoma filtration. In such procedures, the high viscosity of hyaluronan is used to maintain the intraocular space and so allow the manipulation of tissues, while its viscoelastic behaviour is of importance for the protection of ocular cells and tissues. Knowledge of the properties of such preparations under shear is of direct relevance to understanding the physical processes occurring when the solution is injected through a cannula, during movement of surgical instruments within the solution and

* Corresponding author. Tel.: +46-18-671-553; fax: +46-18-673-477.
E-mail address: sally.harding@kemi.slu.se (S.G. Harding).

0144-8617/02/$ - see front matter
PII: S0144-8617(01)00183-7

in the turbulent flow conditions occurring during modern cataract extraction (phacoemulsification) procedures.

In recent years, NMR velocity imaging (velocimetry) has been employed to study the rheometric characteristics of complex fluids under shearing flows — an area of research often referred to as 'rheo-NMR' (Callaghan, 1999). A wide variety of complex fluids have been examined including, for example; a variety of food systems (Britton & Callaghan, 1997), particulate suspensions (Mc Carthy & Kerr, 1998) and polymer solutions (Xia & Callaghan, 1990). In addition to pipe flow geometry velocity imaging has also been used in conjunction with a concentric cylindrical couette cell, the cone and plate cell and the four-roll mill (Britton, Callaghan, Kilfoil, Mair & Owens, 1998; Hanlon, Gibbs, Hall, Haycock, Frith, Ablett et al., 1998). Rheo-NMR has proven to be of considerable value for studying a variety of flow behaviours during pipe flow, including shear thinning, plug flow-spurt effects, wall slip and shear banding. Shear thinning behaviour has been observed in various systems including poly(ethylene oxide), poly(acrylamide) and xanthan gum solutions (Arola, Powell, Barrall & McCarthy, 1999; Gibbs, James, Hall, Haycock, Frith & Ablett, 1996; Xia & Callaghan, 1991). Shear thinning results from alignment of molecules in the flow direction causing a decrease in viscosity with increasing shear rate. Wall slip effects have been observed for agar gel particles (Gibbs et al., 1996) and some batches of xanthan solutions (Rofe, de Vargas, Perez-Gonzalez, Lambert & Callaghan, 1996). Wall slip effects have been associated with disentanglement effects at the wall surface. In a series of papers (Britton, Mair, Lambert & Callaghan, 1999; Callaghan, Cates, Rofe & Smeulders, 1996; Mair & Callaghan, 1996, 1997) the rheology of wormlike micellar solutions has been explored using rheo-NMR. The authors observed a transition from Newtonian behaviour to wall slip to unstable flow to shear banding with increasing apparent shear rate and surfactant concentration. The unstable flow and shear banding effects were attributed to inflections in the flow curve giving rise to multiple values of shear stress for a certain range of shear rate values around the inflection point.

In this article we report the first NMR velocity imaging study of the pipe flow behaviour of the important polysaccharide — hyaluronan. In particular the effect of varying concentration and weight average molecular weight, $\bar{M}_w$, on the flow behaviour is investigated.

2. Experimental

2.1. Samples

Three commercially available hyaluronan solutions used as ophthalmosurgical aids were supplied by Pharmacia and Upjohn AB; Healon® (concentration 10 mg ml^{-1}, $\bar{M}_w$ 5×10^6), Healon® GV (concentration 14 mg ml^{-1}, $\bar{M}_w$ 7×10^6) and Healon®5 (concentration 25 mg ml^{-1}, $\bar{M}_w$ 5×10^6). Samples with M_w of 5.3, 3.2, 1.8, 0.6, and 0.3×10^6 were produced by extensive heat degradation at 128°C of a Healon®5 solution (concentration 23 mg ml^{-1}, $\bar{M}_w$ 5.3×10^6).[1] The weight average molecular weights, $\bar{M}_w$s were determined by low angle laser light scattering. These samples were then diluted to give solutions with concentrations 23, 17, 15, 7 and 1 mg ml^{-1}. Dilutions were performed by weighing and using a phosphate buffered saline (0.002 M Na-phosphate in 0.145 M NaCl, pH 7.3) as solvent. The diluted samples were mixed in a vortex mixer for 1 h and then with magnetic stirrer overnight before being stored at 4°C for up to one week prior to the imaging experiments.

2.2. Rheometry

The rheological properties of the solutions were evaluated by measuring the steady shear viscosity on a Bohlin VOR Rheometer (Bohlin Reologi AB, Lund, Sweden). All measurements were performed at 25°C with a concentric cylinder (cup and bob) system.

2.3. NMR velocity imaging

The practical and theoretical details of the NMR methods employed in this work have been described in detail in several texts including (Callaghan, 1991, 1999). The method involves acquisition of the 'dynamic displacement profile' in each spatially localised region. This method not only gives the average velocity in each spatial region from the centre of the dynamic displacement profile but also provides a check on flow stability and the distribution of flows within each region. In this method the velocity data is obtained by acquiring a succession of NMR images or profiles in which the two magnetic field gradients of duration δ and separation Δ used to encode for velocity are successively stepped in magnitude, in n_D increments up to a maximum value g_m. The data set is then Fourier analysed to provide a dynamic displacement profile consisting of N points describing the motion in each pixel of the image. The average velocity, v, for each pixel is then calculated by fitting a gaussian function to the dynamic displacement profile to find the peak centre at a digital value k_v.

$$v = \frac{2\pi n_D k_v}{N\gamma\delta\Delta g_m}. \quad (1)$$

The radial velocity profiles were obtained from two types of data: by radial averaging two dimensional (2D) velocity maps of a horizontal cross-sectional slice and by inverse Abel transformation of one dimensional (1D) transverse profiles. The 2D imaging technique can be regarded as the benchmark method for NMR capillary velocity imaging and provides unambiguous velocity data and a check on the assumed axial symmetry of the system. The 1D profiling technique has been demonstrated

[1] Both Healon®5 samples fall within the product specification.

by Gibbs, Haycock, Frith, Ablett and Hall (1997) as an alternative technique that is potentially much quicker, and could, for example be useful to follow changes in the flow pattern over time.

The solution was pumped through a 3 m length of PTFE (Teflon) tubing using a Pharmacia (P-500) pump to control the flow rate. The PTFE tubing was of internal diameter 2.56 or 1.52 mm. The tubing was aligned vertically through the bore of the magnet and held in position using a thicker Teflon sleeve as it passed through the gradient coils and the imaging region. Velocity profiles were obtained for flows ranging from 0 to 45 ml h^{-1} (typically at the values 0, 5, 10, 15, 30 and 45 ml h^{-1}).

All measurements were acquired using a Bruker DRX 600 NMR spectrometer with micro imaging accessories. Typical acquisition conditions involved a spectral width of 40,000 Hz and a slice thickness of 1 mm. 2D images were acquired with an image array of 128^2 points giving a spatial resolution of 23 or 14 μm $pixel^{-1}$ for flow through the 2.56 mm and 1.52 mm diameter tubing, respectively. 1D profiles were acquired with a data size of 256 points giving spatial resolutions of 12 and 7 μm $pixel^{-1}$ for flow though the larger and smaller diameter tubing, respectively. The velocity phase encoding time was typically 20–50 ms. The flow gradient duration, δ was 0.5 ms, the strength of the flow gradient was incremented from 0 to 117.6 G cm^{-1}, and the gradient separation time, Δ was typically 30 ms. The 2D slice selective flow images were acquired using a repetition time of 300 ms and two co-additions giving a total acquisition time of 10 min 15 s. The 1D profiles were acquired with a repetition time of 4 s and 4 co-additions giving a total acquisition time 2 min 20 s.

The 2D slice selective images were Fourier transformed in both the two spatial dimensions and the flow dimension using 'XwinNMR' software. The data was then transferred to MATLAB for further processing. The velocity in each pixel of the image was determined from the dynamic displacement profiles by fitting to a gaussian function and using Eq. (1). Radial averaged profiles were calculated from the 2D velocity images by averaging pixels within a specified radial interval from the centre of the image, for all such radial intervals. The 'x–y' co-ordinates of the centre of the image were determined from the total intensity image by fitting the projections of the image in the x and y directions to equations for the projection of a circle onto a line. The 1D profiles were Fourier transformed only in the spatial domain using XwinNMR software before being transferred to MATLAB where the profiles were transformed to radial profiles using the discrete inverse Abel transform DIAT as implemented and described in detail by Gibbs et al. (1997). These profiles were then Fourier transformed to produce a propagator for each radial position and the velocity calculated from the propagator in an analogous way to that used for the 2D images.

2.4. Flow in pipe geometry

In the NMR imaging experiment, when studying flows in pipe geometry, the velocity profile, $v(r)$, as a function of the radial distance, r, from the centre of the pipe is measured. The radial dependence of the shear stress in such a geometry allows determination of the form of the flow curve — shear stress, σ, verses shear rate, $\dot{\gamma}$, form the velocity profile. The shear rate, $\dot{\gamma}$, is calculated by taking the derivative of the velocity profile,

$$\dot{\gamma} = \frac{\partial \gamma}{\partial t} = -\frac{\partial v(r)}{\partial r}. \tag{2}$$

If the pressure drop, ΔP, per unit length of the tube is also known the shear stress at each radial position can be calculated from

$$\sigma = \frac{r\Delta P}{2}. \tag{3}$$

In the work reported here, the pressure drop could not be measured and so the shear stress axis is arbitrarily scaled. Comparison of the flow curve determined from the rheometric viscosity with the form of the flow curve derived from the radial velocity profiles can be used to determine the scaling factor ($\Delta P/2$) —a method previously applied by Rofe et al. (1996). To aid the comparison of the velocity profiles acquired for flow through the two tubes with different radii the definition of apparent shear rate $\dot{\gamma}_{app}$ at the flow rate, Q, is used and defined by

$$\dot{\gamma}_{app} = \frac{4Q}{\pi a^3}, \tag{4}$$

where a is the tube radius. For a solution in which the viscosity is independent of shear rate (described as Newtonian) the radial variation of velocity will be parabolic and described by the equation

$$v(r) = v_{max}\left[1 - \left(\frac{r}{a}\right)^2\right], \tag{5}$$

where a is the pipe radius and $v(r)$ is the velocity at radius r. Many dilute polymer solutions display shear thinning behaviour and are described by a power law relationship between shear rate, $\dot{\gamma}$, and shear stress, σ,

$$\frac{\partial \gamma}{\partial t} = \phi\sigma^N, \tag{6}$$

where $N > 1$ and ϕ is a constant. The radial variation in velocity, $v(r)$, is then described by the equation

$$v(r) = v_{max}\left[1 - \left(\frac{r}{a}\right)^{(N+1/N)}\right]. \tag{7}$$

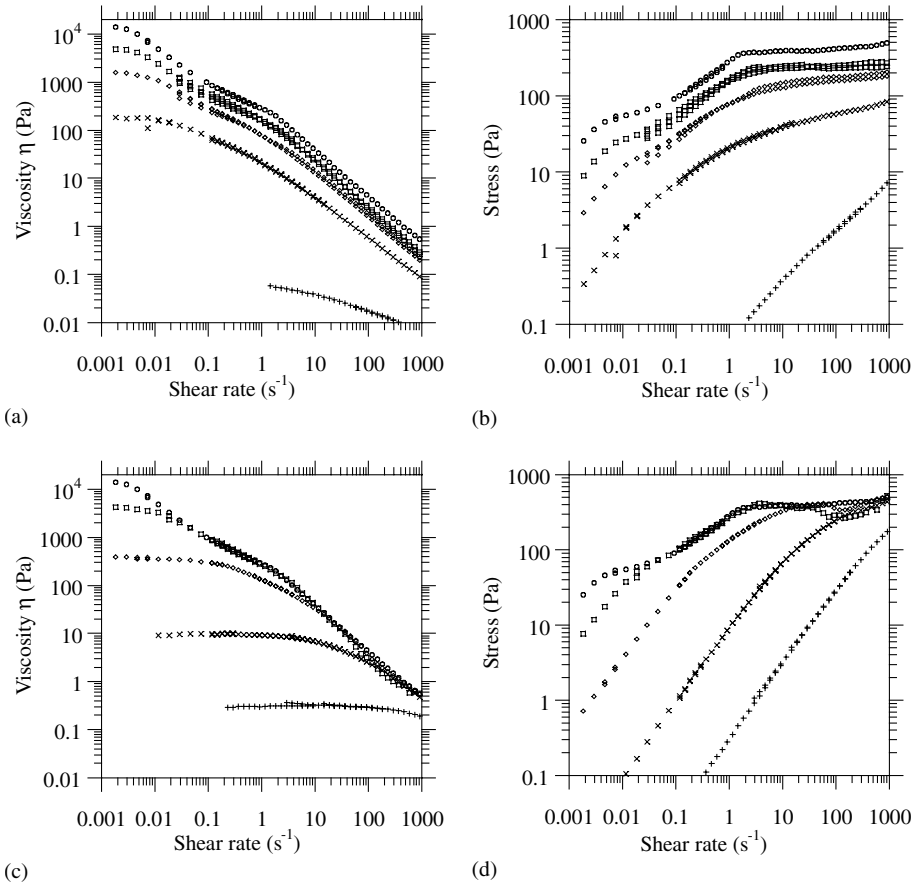

Fig. 1. Rheometric viscometry of hyaluronan solutions. (a) Viscosity against shear rate for hyaluronan of $\bar{M}_w$ 5.3×10^6 and concentrations of (○) 23, (□) 17, (◇) 15, (×) 7 and (+) 1 mg ml^{-1}. (b) Flow curve (sheer stress against shear rate) for the same samples as in (a). (c) Viscosity against shear rate for hyaluronan of concentration 23 mg ml^{-1} and $\bar{M}_w$ (○) 5.3, (□) 3.2, (◇) 1.8, (×) 0.6 and (+) 0.3×10^6. (d) Flow curve (sheer stress against shear rate) for the same samples as in (c).

3. Results

3.1. Rheometry

The rheological properties of the solutions determined from the viscosity measurements are shown in Fig. 1 for a representative selection of the samples studied. The shear rate dependence of viscosity is shown in Fig. 1(a) for samples with the same $\bar{M}_w$ and varying concentration and in Fig. 1(c) for samples with the same concentration and varying $\bar{M}_w$. Fig. 1(b) and (d) show the corresponding data for the two sets of samples plotted in the form of a flow curve. In this form the data can be directly compared with the flow curves derived from the NMR imaging velocity profiles using Eqs. (2) and (3). The solutions show a behaviour typical of high $\bar{M}_w$ polymer solutions and are in accordance with the results reported by Bothner & Wik (1989), Bothner et al. (1988). At low shear rates the disruption of existing entanglements by the imposed flow is balanced by the formation of new entanglements and the solutions exhibit Newtonian behaviour — the viscosity remains constant. At higher shear rates the reentanglements can no longer keep pace with the forced disentanglements and viscosity falls. The onset of shear thinning behaviour moves to higher shear rates with decreasing polymer $\bar{M}_w$ and concentration. In the limit of high shear rate the viscosity is approximately independent of $\bar{M}_w$ as shown by the convergence of the data at high shear rates in Fig. 1(c) and (d). The plots of viscosity against shear rate (especially for samples at the highest concentrations and $\bar{M}_w$s) show a series of 'steps' which correspond to varying power law exponents, N, as defined in Eq. (6). Samples with high $\bar{M}_w$s and concentrations show

Table 1
Summary of the flow behaviour of the set of prepared hyaluronan samples with varying concentrations and $\bar{M}_w$s. The flow behaviour is grouped into; N — Newtonian, ST — shear thinning, ST^p — shear thinning obeying power law dependence, AS — apparent slip and SB — shear banding

Hyaluronan concentration (mg ml^{-1})	Weight average molecular weight, $\bar{M}_w$ ($\times 10^6$)				
	5.3	3.2	1.8	0.6	0.3
23	SB	AS	ST	ST	N
17	AS	AS	ST	ST	N
15	AS	ST	ST	ST^p	N
7	ST	ST	ST	N	N
1	ST^p	ST^p	N	N	N

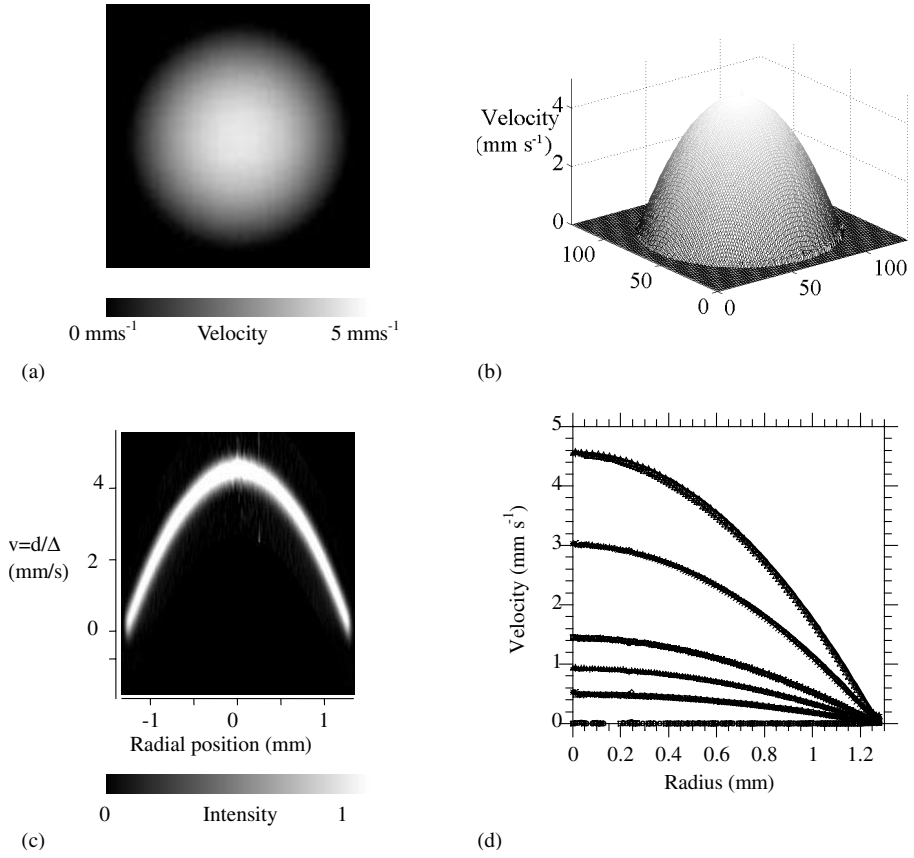

Fig. 2. Velocity images for flow of hyaluronan (concentration 7 mg ml^{-1}, $\bar{M}_w$ 0.6×10^6) through a Teflon tube of internal diameter 2.56 mm. (a) 2D velocity image of horizontal cross-section at a flow rate of 45 ml h^{-1}. Velocities represented on the grey-scale as indicated in the figure. (b) Same data as in (a) represented as a mesh plot. (c) 1D velocity profile after inverse Abel transform showing dynamic displacement profiles for each spatial position at a flow rate of 45 ml h^{-1}. The scale in the displacement direction is shown in terms of displacement, d, divided by velocity encoding time, Δ, to allow direct comparison with velocity plots. Grey-scale indicates intensities. (d) Velocity profiles calculated by radial averaging of velocity images and inverse Abel transformation of 1D profiles for flow rates of (○) 0, (□) 5, (◇) 10, (×) 15, (+) 30 and (△) 45 ml h^{-1}. The solid line shows the fit of Eq. (5) for parabolic Newtonian flow to the data.

a plateau in shear stress above a critical shear rate — in this region the stress is roughly independent of shear rate. Some samples, for example (concentration 23 mg ml^{-1} and $\bar{M}_w$ 3.2×10^6 and 1.8×10^6) show some evidence of a decrease in stress at shear rates in excess of around 50 s^{-1}.

3.2. NMR velocity imaging

Based on the velocity profiles obtained for the hyaluronan solutions studied four distinct types of flow behaviour are discernible. The flow behaviour found in the set of prepared samples with varying concentrations and $\bar{M}_w$s is summarised in Table 1. The low molecular weight — low concentration samples show profiles typical of Newtonian flow. As the concentration or $\bar{M}_w$ is increased a transition is observed to profiles characteristic of a shear thinning solution — this type of profile is also found for the Healon® sample. Those samples in which all profiles are well fitted by a power law relationship between shear rate and strain are indicated in the table. As concentration or $\bar{M}_w$ is increased still further some samples show a non zero velocity at the tube wall characteristic of wall slip. Wall slip characteristics are also seen in the Healon® GV sample. Finally the solution with the highest concentration and $\bar{M}_w$ (concentration 23 mg ml^{-1} and $\bar{M}_w$ 5.3×10^6 Da) and Healon®5 shows possible evidence for shear banding effects. These four regimes are described in more detail in the following sections.

3.3. Newtonian flow

Typical results for a solution displaying Newtonian flow characteristics are shown in Fig. 2. Fig. 2(a) and (b) show the results of the 2D velocity image of a horizontal cross-section through the tube for a flow rate of 45 ml h^{-1} in the form of (a) a grey-scale image and (b) a mesh plot. The flow rate reported was the flow rate setting of the pump during the experiment — however the flow rate can also be directly calculated from the image by taking the average velocity measured in the velocity image. For the data shown in Fig. 2(a) and (b) such a calculation results in a flow rate of 44.85 ± 0.05 ml h^{-1} compared to the flow reading of 45 ml h^{-1}. The error is estimated by comparing the calculated flow rates from the velocity image and the velocity

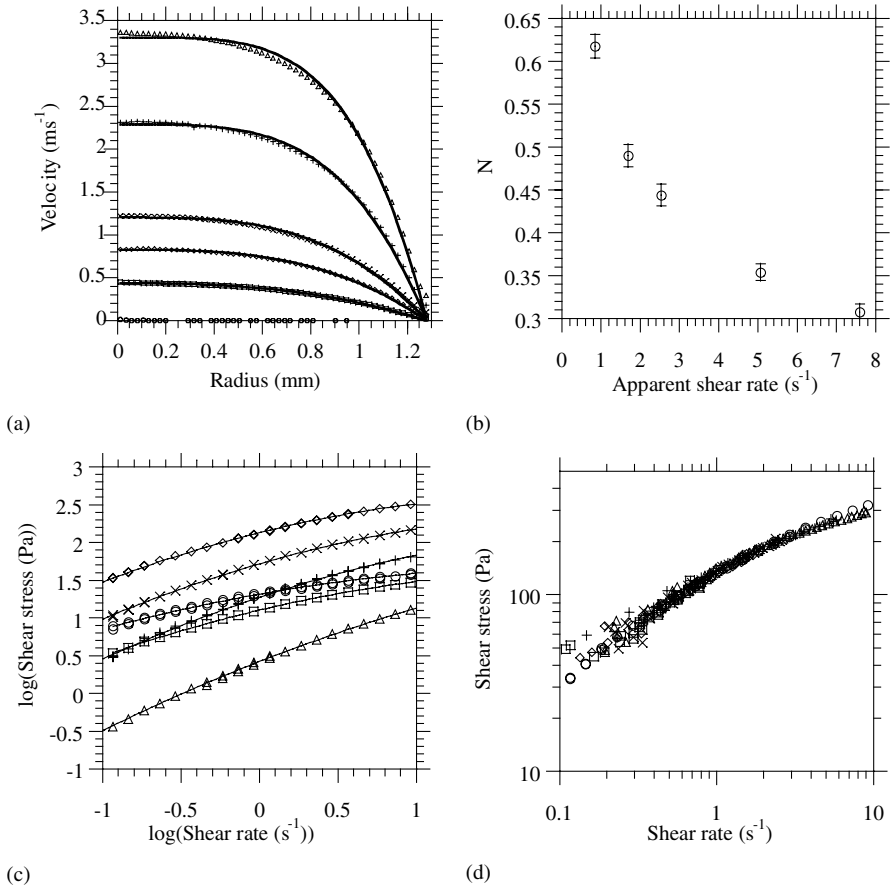

Fig. 3. (a) Velocity profiles for flow of hyaluronan (concentration 23 mg ml^{-1}, $\bar{M}_w$ 1.8×10^6) through a Teflon tube of internal diameter 2.56 mm for flow rates of (○) 0, (□) 5, (◇) 10, (×) 15, (+) 30 and (△) 45 ml h^{-1}. The solid lines show the fit of Eq. (7) (describing the velocity profiles when there is a power law dependence of shear stress against shear rate) to the data. (b) The power law exponent, N, (defined in Eq. (6)) determined from the fit of Eq. (7) to the data shown in (a) against the apparent shear rate, $\dot{\gamma}_{app}$. (c) Flow curve for hyaluronan solutions displaying sheer thinning behaviour; (○) 7 mg ml^{-1}, $\bar{M}_w$ 5.3×10^6, (□) 7 mg ml^{-1} $\bar{M}_w$ 3.2×10^6, (◇) 23 mg ml^{-1}, $\bar{M}_w$ 1.8×10^6, (×) 17 mg ml^{-1}, $\bar{M}_w$ 1.8×10^6, (+) 15 mg ml^{-1}, $\bar{M}_w$ 1.8×10^6, (△) 7 mg ml^{-1}, $\bar{M}_w$ 1.8×10^6. The solid lines show a polynomial fit of the logarithmic data. (d) Sheer stress verses shear rate for $\bar{M}_w$ hyaluronan (concentration 23 mg ml^{-1}, $\bar{M}_w$ 1.8 — $\bar{M}_w$ $\times 10^6$ (○) from rheometry and from velocity images at flow rates of (□) 5, (◇) 10, (×) 15, (+) 30 and (△) 45 ml h^{-1}.

image after removal of the outer layer of pixels at the edge of the tube. This estimation allows the fact that the outer pixels will only be partly liquid filled to be taken into account. Fig. 2(c) shows the results of the 1D profiling experiment for the same sample at the same flow rate. The image shows the dynamic displacement profiles at each radial location calculated from the raw data by the inverse Abel transform routine prior to Fourier transformation in the velocity direction. Fig. 2(d) shows the radial profiles obtained for this solution at a range of flow rates. The data shown has been calculated from both 2D velocity images and 1D profiles. The standard deviation of the velocity values in each radial group has a mean value, (averaged over all radial groups examined) of 0.07 mm s^{-1}. Agreement between the 1D profiling and 2D imaging methods appears to be very good and for flow at 45 ml h^{-1} the correlation coefficient for the two sets of data is 0.9996. On the same plot is shown a fit of the data to parabolic velocity profiles (Eq. (5)) expected for a Newtonian fluid. Again the agreement between the predicted and measured data appears to be very good with, for the 45 ml h^{-1}, flow rate a regression coefficient of 0.9995. All samples displaying Newtonian flow characteristics in the NMR velocity profiles were also characterised by a slope of 1 on a logarithmic plot of shear stress against shear rate ($N = 1$, according to Eq. (5)) determined from the viscosity measurements over the range of shear rates experienced in the pipe flow.

3.4. Shear thinning

The Healon® solution and hyaluronan solutions with intermediate concentrations and $\bar{M}_w$s gave profiles that were somewhat blunter than the ideal parabolic profile of a Newtonian fluid indicative of a shear thinning solution, in which the viscosity decreases with increasing shear rate. This type of regime may be expected as shearing will reduce the effects of polymer — polymer contacts or entanglements, so decreasing the solution viscosity. Fig. 3(a) shows radial velocity profiles for flow of hyaluronan (concentration 23 mg ml^{-1}, $\bar{M}_w$ 1.8×10^6) through Teflon

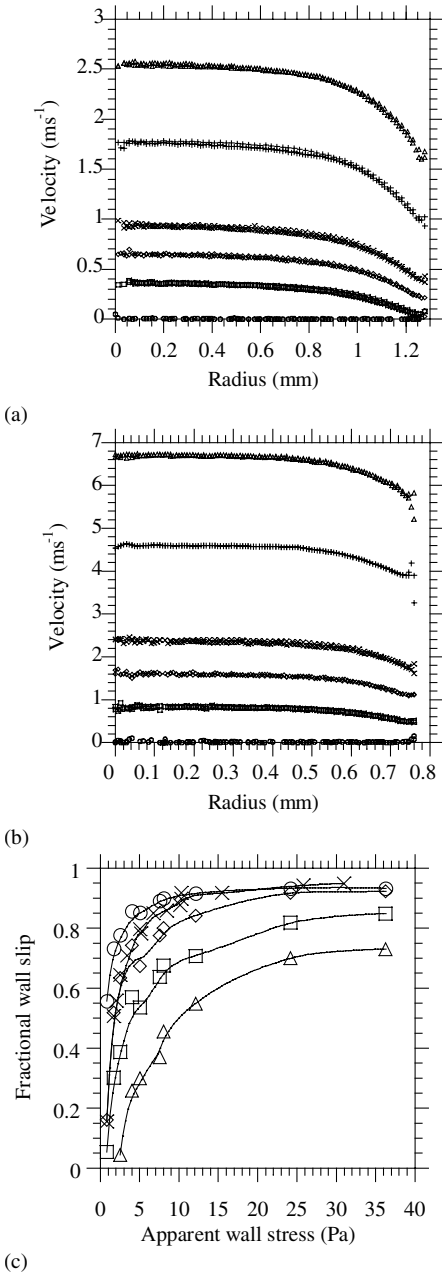

Fig. 4. (a) Velocity profiles for flow of hyaluronan (concentration 15 mg ml^{-1}, $\bar{M}_w$ 5.3×10^6) through Teflon tube of internal diameter 2.56 mm for flow rates (○) 0, (□) 5, (◇) 10, (×) 15, (+) 30 and (△) 45 ml h^{-1}. (b) Same as (a) for flow through tube of internal diameter 1.52 mm. (c) Fractional wall slip against apparent wall stress for hyaluronan solutions (○)17 mg ml^{-1}, $\bar{M}_w$ 5.3×10^6, (□) 15 mg ml^{-1}, $\bar{M}_s$ 5.3×10^6, (◇) 23 mg ml^{-1}, $\bar{M}_w$ 3.2×10^6 and (×)17 mg ml^{-1}, $\bar{M}_w$ 3.2×10^6.

tube of internal diameter 2.56 mm — these profiles are typical of profiles displaying shear thinning characteristics. Fig. 3(a) also shows the fit of the velocity profiles to Eq. (7) assuming a power law relationship between shear strain and shear rate, as shown in Eq. (6). Although each individual profile could be fitted by this equation with a R^2 coefficient of around 0.996, the fitted value of N was found to increase with the flow rate, as shown in Fig. 3(b). This indicates that the power law model (Eqs. (6) and (7)) does not accurately describe the flow of this hyaluronan solution over the range of flow rates studied in the experiments. This result is supported by examination of the viscosity measurements over the range of shear rates between 0.1 and 10 typical of those found in the imaging studies. Plotted on logarithmic scales there is a curvature in the relationship between shear stress and shear rate for these solutions as shown in Fig. 3(c). The shear stress axis of the flow curves derived from the NMR velocity profiles were quantified by comparison with the flow curve from the viscometry measurements. The flow curve from the viscometry measurements was fitted by a polynomial on logarithmic scales, as shown by the solid lines in Fig. 3(c). By fitting the same equation to the NMR derived flow curve the scaling of the shear stress axis ($\Delta P/2$) was determined. Fig. 3(d) compares the plots of shear strain against shear rate determined in this manner with the results of viscometry measurements over the range of shear rates found in the imaging experiments. The agreement between the two data can be seen in the shapes of the plots. It should also be noted that some of the solutions displaying shear thinning characteristics were well fitted by the power law model shown in Eq. (6); such samples are indicated in Table 1.

3.5. Wall slip

Healon® GV and four of the samples as indicated in Table 1 showed a non zero velocity at the edge of the tube in addition to shear thinning behaviour. This is symptomatic of wall slip. Radial velocity profiles typical of a solution displaying wall slip behaviour are shown in Fig. 4(a) and (b) for flow of hyaluronan (concentration 15 mg ml^{-1}, $\bar{M}_w$ 5.3×10^6) through Teflon tubing of internal diameter 2.56 mm and 1.52 mm, respectively. For each tube size the fractional wall slip increases with flow rate and this behaviour is highlighted in Fig. 4(c) which shows fractional wall slip as a function of apparent shear stress, calculated using Eq. (4). Values recorded in the two tubes at comparable apparent shear rates show good agreement. The fractional wall slip was calculated by fitting each profile by Eq. (7) with an added constant on the right hand side to take into account the wall slip velocity. The fits of this equation are shown by solid lines in Fig. 4(a) and (b). This fitting procedure gave a good estimate of the wall slip behaviour; despite the slight curvature in the logarithmic flow curve over the appropriate shear rate range. The fitted values for the wall slip were within the standard deviation of the outer pixel value calculated by radial average of the 2D velocity image.

The radial profiles shown in Fig. 4(a) and (b) represent the average velocity of molecules within the corresponding spatially resolved region of the tube. These profiles show that the average velocity within a pixel at the edge of the tube has a non zero value. This value has been averaged over a region of around 10 μm (depending on the spatial

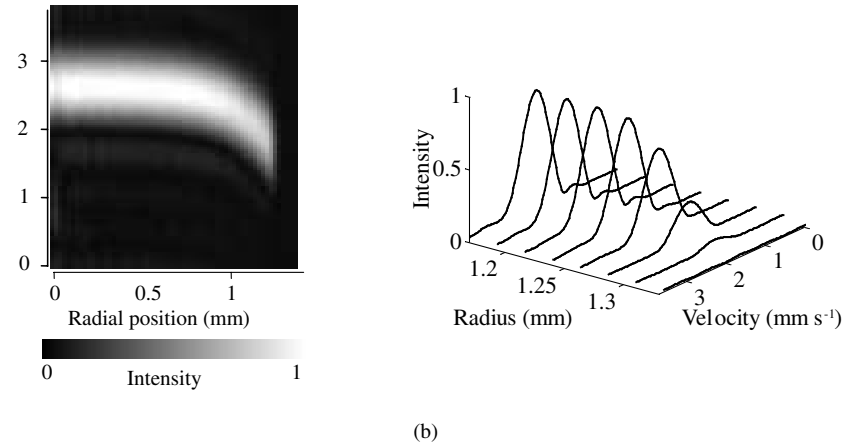

Fig. 5. (a) Dynamic displacement profiles calculated by radial averaging a 2D velocity image for flow of hyaluronan solution (concentration 15 mg ml^{-1}, $\bar{M}_w$ 5.3×10^6) through Teflon tube of internal diameter 2.56 mm. The scale in the displacement direction is shown in terms of displacement, d, divided by velocity encoding time, Δ to allow direct comparison with velocity plots. Grey-scale indicates intensities. (b) Stack plot of data shown in (a) highlighting dynamic displacement profiles at the wall of the Teflon tube.

resolution employed). It can also be instructive however to analyse the dynamic displacement profiles from a spatially resolved region to study the distribution of velocities within that region. Fig. 5(a) and (b) show typical dynamic displacement profiles as a function of radial position for hyaluronan flow showing wall slip effects. By examining these dynamic displacement profiles towards the wall of the tube we can see that within the sensitivity of the dynamic displacement profiles nearest the wall there is no visible component of the liquid with zero velocity over the velocity encoding time, Δ, of 30 ms.

3.6. Apparent shear banding

The Healon®5 samples (concentration 25 mg ml^{-1}, $\bar{M}_w$ 5×10^6 and concentration 23 mg ml^{-1}, $\bar{M}_w$ 5.3×10^6) showed a flat velocity profile across the central region of the tube. Fig. 6(a) and (b) shows radial velocity profiles for flow of hyaluronan (concentration 23 mg ml^{-1}, $\bar{M}_w$ 5.3×10^6) through Teflon tubing of internal diameter 2.56 mm and 1.52 mm, respectively. For flow in the larger tube up to a flow rate of 15 ml h^{-1} ($\dot{\gamma}_{app} = 2.5$ s^{-1}) and in the narrower tube up to a flow rate of 5 ml h^{-1} ($\dot{\gamma}_{app} = 4.0$ s^{-1}) the velocity profiles are flat showing a wall slip behaviour at the edge of the tube. There is no evidence of a high shear rate band or any velocity fluctuations. This is confirmed by examination of the dynamic displacement profiles from the region at the edge of the tube, which show a well-defined gaussian distribution, and no evidence of a zero velocity component. As the flow rate is increased to higher apparent shear rates there appears an outer annulus displaying a well defined lower velocity. This is illustrated in the 2D velocity image shown in Fig. 7(a) and the corresponding dynamic displacement profiles in Fig. 7(b) and (c). The thickness of this annulus is approximately 20–30 μm. As the flow rate is increased still further to 30 ml h^{-1} ($\dot{\gamma}_{app} = 24.2$ s^{-1}) or above in the narrower tube there appears to be a distribution of velocities within this

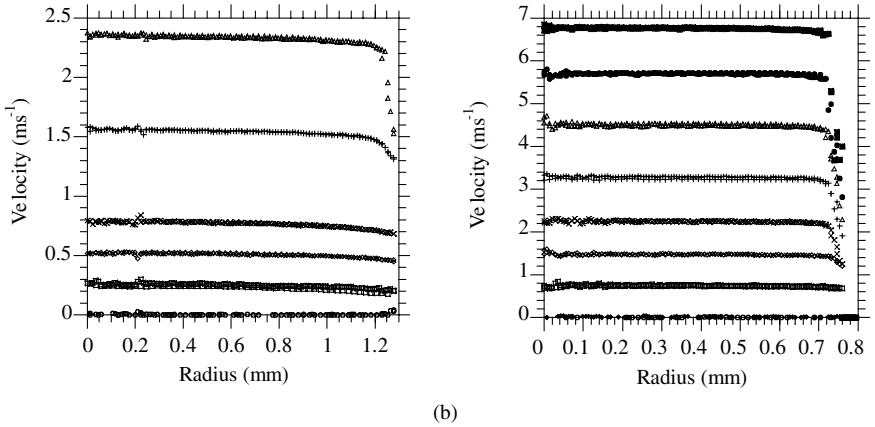

Fig. 6. Velocity profiles for flow of hyaluronan (concentration 23 mg ml, $\bar{M}_w$ 5.3×10^6) through Teflon tube of internal diameter 2.56 mm, for flow rates of (○) 0, (□) 5, (◇) 10, (×) 15, (+) 30 and (△) 45 ml h^{-1}. (b) Same as (a) for flow through tube of internal diameter 1.52 mm, for flow rates of (○) 0, (□) 5, (◇) 10, (×) 15, (+) 22, (△) 30, (●) 38 and (■) 45 ml h^{-1}.

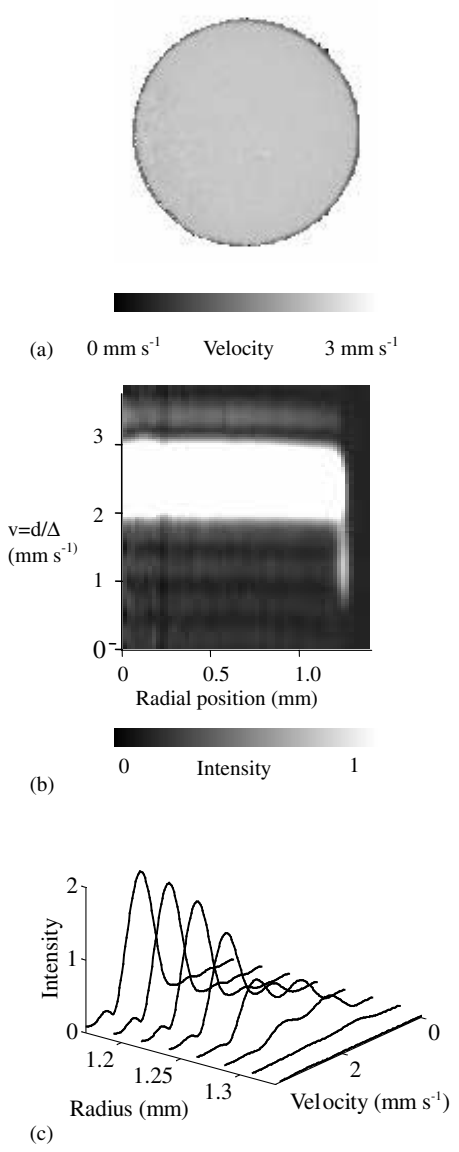

Fig. 7. Velocity images for flow of hyaluronan solutions (concentration 23 mg ml, $\bar{M}_w$ 5.3×10^6) through Teflon tube of internal diameter 2.56 mm, at a flow rate of 45 ml h^{-1}. (a) 2D velocity image of horizontal cross-section. Velocities represented on the grey-scale as indicated in the figure. (b) Dynamic displacement profiles calculated by radial averaging of 2D velocity. The scale in the displacement direction is shown in terms of displacement, d, divided by velocity encoding time, Δ to allow direct comparison with velocity plots. Grey-scale indicates intensities. (c) Stack plot of data shown in (b) highlighting propagators at the edge of the Teflon tube.

outer annulus from 2 mm s^{-1} to the velocity of the central plug. The width of this region of perturbed flow increases with increasing flow rate and is approximately 40–50 μm wide at the highest shear rate studied. This phenomenon is illustrated in Fig. 8. Fig. 8(a) and (b) compare the outer dynamic displacement profiles for a flow rate of 15 ml h^{-1} ($\dot{\gamma}_{app}$= 12.1 s^{-1}) and 38 ml h^{-1} ($\dot{\gamma}_{app}$= 30.6 s^{-1}), respectively. Fig. 8(c) compares the dynamic displacement profiles 40 μm from the outer surface with increasing flow rate.

4. Discussion

All NMR measurements showed good agreement between the 2D velocity imaging and the 1D profiling technique. The 2D imaging technique has the advantage of providing a check on the symmetry of the system while the 1D profiling technique allows faster data acquisition and thus a finer spatial resolution is made possible. The samples displaying Newtonian flow characteristics served as a good standard to estimate the precision and accuracy of the measurement technique. Solutions showing Newtonian characteristics measured by rheometric viscometry over the range of shear rates experienced in the imaging experiments were well fitted by Eq. (5) describing the parabolic velocity profile for a Newtonian fluid. Similarly, solutions displaying shear thinning characteristics showed good agreement between the shape of the flow curves determined from the velocity profiles and rheometric viscometry. It is important to note that for these systems the NMR velocity experiments essentially showed no features that could not be directly inferred from conventional rheometry. The NMR imaging technique is unique, however, in that the distribution of velocities during flow can be directly measured thus allowing hysteresis in the flow behaviour and surface phenomena to be directly visualised. This allowed solutions showing wall slip and possible shear banding phenomena to be directly identified.

Wall slip has previously been observed by NMR velocity imaging (Gibbs et al., 1996; Rofe et al., 1996). In this current study Healon® GV and four of the prepared hyaluronan solutions with high concentration and $\bar{M}_w$ showed evidence of wall slip. Examination of the dynamic displacement profiles from regions at the edge of the tube showed a well-defined gaussian distribution centre significantly above zero velocity. There was no evidence for fluid with zero velocity at the edge of the tube. Therefore the wall slip observed appears to be definitely a surface phenomena — resulting from a modification of fluid properties due to the proximity of a solid surface rather than a consequence of the constitutive relationship describing the bulk rheological properties of the sample. This type of behaviour may be contrasted with the results obtained on Helon®5 solutions. Both these samples showed a transition, with increasing apparent shear rate, from wall slip behaviour to the existence of a boundary layer at a finite velocity to an apparent shear band at the wall. Examination of the dynamic displacement profiles associated with the outer region of the tube showed no evidence of components of flow with velocities less than a certain value (2 mm s^{-1}). A distribution of velocities from 2 mm s^{-1} to the velocity of the central plug was apparent. The width of this perturbed region increased with increasing apparent shear rate. It is unclear whether this apparent shear band results from fluctuations in velocity within the total experiment time (in the order of minutes), fluctuations within the velocity encoding time Δ (30 ms), or whether it is due to the co-existence of velocities within the

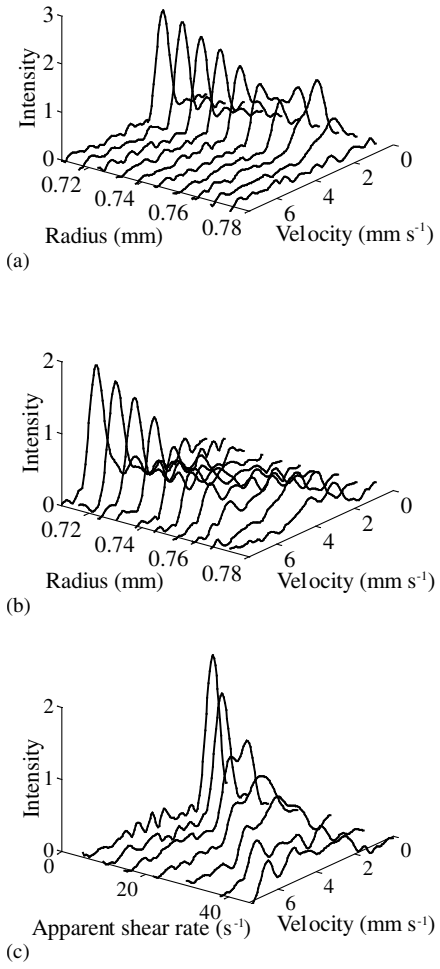

Fig. 8. Dynamic displacement profiles calculated from profiles after inverse Abel transform for flow of hyaluronan (concentration 23 mg ml, $\bar{M}_w$ 5.3×10^6) through Teflon tube of internal diameter 1.52 mm, showing region at the edge of the Teflon tube for a flow rate of (a) 5 ml h^{-1} and (b) 38 ml h^{-1}. (c) Comparison of dynamic displacement profiles approximately 30 μm from edge of Teflon wall at varying apparent shear rates.

spatially resolved volume element. From a microscopic viewpoint the discontinuities in the flow curve may be due to a highly aligned phase adjacent to a less aligned phase. This phenomenon is however distinct from the wall slip feature seen for some other hyaluronan. Similar profiles have been observed for wormlike micelles (Britton et al., 1999; Callaghan et al., 1996; Mair et al., 1996, 1997). The study of Britton et al. (1999) reported the existence of a boundary layer of fluid at a low but finite velocity — a phenomenon seen for the hyaluronan profiles at intermediate apparent shear rates — but the authors could find no physical explanation for such behaviour. In the micellar solutions studied by Britton et al. (1999) the apparent shear banding was attributed to inflections in the flow curves describing the bulk rheological properties of the sample. In pipe flow, for certain flow rates, such an inflection in the flow curve would give rise to a region of high shear in the vicinity of the wall where the stress is highest and the fluid behaviour is characteristic of the upper branch upturn and a low shear region in the centre where the stress is lower. The theoretical basis for the existence of inflections in the flow curve characterising a fluid is however highly dependent upon the relaxation times characterising the molecular motion (Doi & Edwards, 1986; McLeish & Ball, 1986). In wormlike micelles these relaxation processes are averaged by a breakage-recombination process leading to sharply defined effective relaxation times. In contrast, in polymer solutions such as the hyaluronan solutions studied here, the chain length polydispersity is believed to result in a wide spectrum of relaxation times to mask this phenomenon. Thus the explanation in terms of discontinuities in the flow curve may not be a suitable explanation for the results reported here. The high concentration, high $\bar{M}_w$ hyaluronan solutions do however display a wide stress plateau (constant shear stress with increasing shear rate) over the range of shear rates that would be experienced in the pipe flow experiments, as shown in Fig. 1(b) and (d). Some samples (for example, concentration 23 mg ml^{-1}, $\bar{M}_w$ 3.2×10^6) show an inflection in the flow curve at high shear rates (around 100 s^{-1}). This is evidence to support the possibility that the velocity profiles seen for these very high concentration and $\bar{M}_w$ hyaluronan solutions are related to the effects previously observed for wormlike micelles.

5. Conclusions

This study has demonstrated the ability of the NMR velocity imaging technique to investigate the flow behaviour of hyaluronan solutions in pipe flow. The hyaluronan solutions showed a transition from Newtonian behaviour to shear thinning to wall slip to apparent shear banding with increasing concentration and $\bar{M}_w$. A distinct advantage of the NMR velocity imaging technique lies in the ability to directly visualise flow hysteresis and wall slip phenomenon. It has been shown that hyaluronan solutions with concentrations above 15–17 mg ml^{-1} and $\bar{M}_w$ above 3.2×10^6 and Healon® GV can exhibit wall slip behaviour in a PTFE tube. Our results demonstrate that this is very much a surface phenomena. This behaviour can be distinguished from that seen for the Healon®5 solutions. These samples show wall slip behaviour, however, the perturbation at the wall extends a significant distance into the bulk of the fluid. This raises the possibility that this additional perturbation is not a surface phenomenon but rather a property associated with the bulk constitutive equation of the solution. This feature has therefore been described as apparent shear banding. A similar effect has previously been reported by Britton et al. (1999) for a wormlike micellar solution, however the results reported in this present study represent the first demonstration of such possible effects for dilute polymer solutions. The possibility of shear banding effects has important implications from a theoretical viewpoint in our understanding of the behaviour under shear of random coil polymers. It also has very practical applications concerning

the formulation of ophthalmosurgical aids with the desired shear behaviour.

Acknowledgements

Sally G. Harding gratefully acknowledges Pharmacia and Upjohn for financial support. The authors are grateful to Rolf Hjorth and Lars Hagel for valuable comments on the manuscript.

References

AlAssaf, S., Meadows, J., Phillips, G. O., & Williams, P. A. (1996). The application of shear and extensional viscosity measurements to assess the potential of hylan in viscosupplementation. *Biorheology*, *33* (4/5), 319–332.

Ambrosio, L. A., Borzacchiello, P. A., Netti, P. A., & Nicolais, L. (1999). Properties of new materials: rheological study on hyaluronic acid and its derivative solutions. *JMS-Pure and Applied Chemistry*, *A36* (7/8), 991–1000.

Arola, D. F., Powell, R. L., Barrall, G. A., & McCarthy, M. J. (1999). Pointwise observations for rheological characterization using nuclear magnetic resonance imaging. *Journal of Rheology*, *43* (1), 9–30.

Britton, M., & Callaghan, P. T. (1997). NMR microscopy and the non-linear rheology of food materials. *Magnetic Resonance in Chemistry*, *35*, S37–S46.

Britton, M. M., Callaghan, P. T., Kilfoil, M. L., Mair, R. W., & Owens, K. M. (1998). NMR velocimetry and spectroscopy at microscopic resolution in small rheometric devices. *Applied Magnetic Resonance*, *15* (3/4), 287–301.

Britton, M. M., Mair, R. W., Lambert, R. K., & Callaghan, P. T. (1999). Transition to shear banding in pipe and Couette flow of worm-like micellar solutions. *Journal of Rheology*, *43* (4), 897–909.

Bothner, H., & Wik, O. (1989). Rheology of intraocular solutions. In S. Rosen, *Viscoelastic materials. Basic principles and clinical applications* (pp. 3–22). New York: Pergamon Press.

Bothner, H., Waaler, T., & Wik, O. (1988). Limiting viscosity number and weight average molecular weight of hyaluronate samples produced by heat degradation. *International Journal of Biological Macromolecules*, *10*, 287–291.

Callaghan, P. T. (1991). *Principles of nuclear magnetic resonance microscopy*, London: Oxford University Press.

Callaghan, P. T. (1999). Rheo-NMR: nuclear magnetic resonance and the rheology of complex fluids. *Reports on Progress in Physics*, *62* (4), 599–670.

Callaghan, P. T., Cates, M. E., Rofe, C. J., & Smeulders, J. B. A. F. (1996). A study of the spurt effect in wormlike micelles using nuclear magnetic resonance microscopy. *Journal de Physique II*, *6* (3), 375–393.

Desmedt, S. C., Dekeyser, P., Ribitsch, V., Lauwers, A., & Demeester, J. (1993). Viscoelastic and transient network properties of hyaluronic-acid as a function of the concentration. *Biorheology*, *30* (1), 31–41.

Doi, M., & Edwards, S. F. (1986). *The theory of polymer dynamics*, London: Oxford University Press.

Gibbs, S. J., James, K. L., Hall, L. D., Haycock, D. E., Frith, W. J., & Ablett, S. (1996). Rheometry and detection of apparent wall slip for Poiseuille flow of polymer solutions and particulate dispersions by nuclear magnetic resonance velocimetry. *Journal of Rheology*, *40* (3), 425–440.

Gibbs, J., Haycock, D. E., Frith, W. J., Ablett, S., & Hall, L. D. (1997). Strategies for rapid NMR rheometry by magnetic resonance imaging velocimetry. *Journal of Magnetic Resonance*, *125* (2), 43–51.

Hanlon, A. D., Gibbs, S. J., Hall, L. D., Haycock, D. E., Frith, W. J., Ablett, S., & Marriott, C. (1998). A concentric cylinder Couette flow system for use in magnetic resonance imaging experiments. *Measurement Science and Technology*, *9* (4), 631–637.

Mair, R. W., & Callaghan, P. T. (1996). Observation of shear banding in worm-like micelles by NMR velocity imaging. *Europhysics Letters*, *36* (9), 719–724.

Mair, R. W., & Callaghan, P. T. (1997). Shear flow of worm-like micelles in pipe and cylindrical Couette geometries as studied by nuclear magnetic resonance microscopy. *Journal of Rheology*, *41* (4), 901–924.

McCarthy, K. L., & Kerr, W. L. (1998). Rheological characterization of a model suspension during pipe flow using MRI. *Journal of Food Engineering*, *37* (1), 11–23.

McLeish, T. C. B., & Ball, R. C. (1986). A molecular approach to the spurt effect in polymer melt flow. *Journal of Polymer Science*, *24*, 1735–1745.

Milas, M., Roure, I., & Berry, G. C. (1996). Crossover behaviour in the viscosity of semiflexible polymers: solutions of sodium hyaluronate as a function of concentration, molecular weight, and temperature. *Journal of Rheology*, *40* (6), 1155–1166.

Rofe, C. J., de Vargas, L., Perez-Gonzalez, J., Lambert, R. K., & Callaghan, P. T. (1996). Nuclear magnetic resonance imaging of apparent slip effects in xanthan solutions. *Journal of Rheology*, *40* (6), 1115–1128.

Xia, Y., & Callaghan, P. T. (1990). The measurement of diffusion and flow in polymer-solutions using dynamic NMR microscopy. *Makromolekulare Chemie-Macromolecular Symposia*, *34*, 277–286.

Xia, Y., & Callaghan, P. T. (1991). Study of shear thinning in high polymer-solution using dynamic NMR microscopy. *Macromolecules*, *24* (17), 4777–4786.